Electronic Supplementary Material (ESI) for Chemical Science.
This journal is © The Royal Society of Chemistry 2023

Supporting Information

A Universal Orthogonal Imaging Platform for Living-Cell RNA Detection using Fluorogenic RNA Aptamers

Peng Yin, Mingmin Ge, Shiyi Xie, Li Zhang, Shi Kuang* and Zhou Nie*

State Key Laboratory of Chemo/Biosensing and Chemometrics, College of Chemistry and Chemical Engineering, Hunan University, Changsha, 410082, P. R. China.

*E-mail address: niezhou.hnu@gmail.com (Zhou Nie), kuangshi@hnu.edu.cn (Shi Kuang)

Content

1. Synthesis and Characterization

1.1. Synthesis of 4-((2-hydroxyethyl)(methyl)amino)benzaldehyde(1)(1)

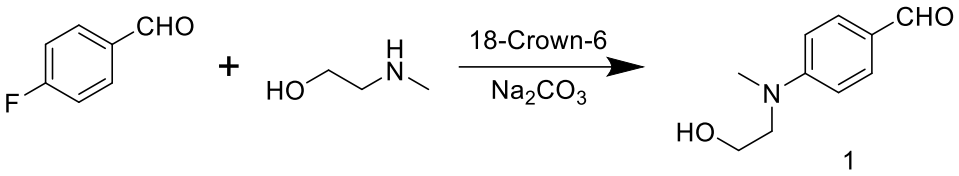

2 mL N-methylaminoethanol (24.2 mmol) was added to a stirred solution of 4-fluorobenzaldehyde (2 g, 16.12 mmol), 18-Crown-6 (82.6 mg, 0.31 mmol) and anhydrous sodium carbonate (3.35g, 24.2 mmol), in 4.5 mL dry DMSO. The mixture was stirred and kept at 100 ℃ for 24 h under N_2. After allowing the reaction to cool to room temperature, the mixture was diluted with 50 mL of ice water and extracted with DCM (50 mL × 3). Then, the organic phase was collected and dried with anhydrous Na_2SO_4 overnight and then concentrated under vacuum to give the crude product, which was then purified by silica gel column chromatography to yield compound **1**(0.9 g, 45%). ^{1}H NMR (400 MHz, $CDCl_3$) δ 9.63 (s, 1H), 7.65 (d, J = 8.8 Hz, 2H), 6.72 (d, J = 8.8 Hz, 2H), 3.85 (t, J = 5.8 Hz, 2H), 3.61 (t, J = 5.8 Hz, 2H), 3.10 (s, 3H).

1.2. Synthesis of (4-((2-hydroxyethyl)(methyl)amino)-benzylidene)-cyanophenylacetonitrile (HBC530)(1)

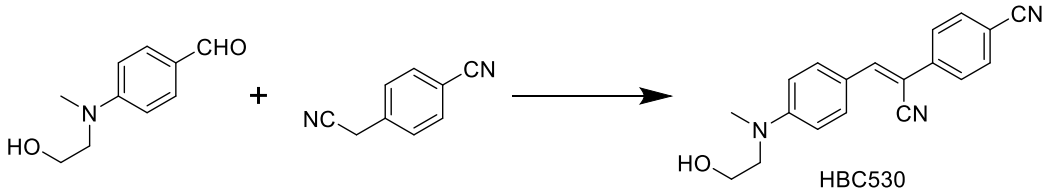

Compound **1** (0.9 g, 5.29 mmol) and 4-cyano-benzeneacetonitrile (0.165g, 1.16 mmol) in 11 mL dry methanol, and two drops of piperidine were added and stirred at room temperature for 1 h. After allowing the reaction to cool to room temperature, the crude

product was purified by silica gel column chromatography (CH_2Cl_2: EtOH = 400:1, v/v) to yield compound HBC530 (0.512g, 57%). ^{1}H NMR (400 MHz, $CDCl_3$) δ 7.88 (d, *J* = 8.8 Hz, 2H), 7.70 (q, *J* = 8.4 Hz, 4H), 7.48 (s, 1H), 6.80 (d, *J* = 8.8 Hz, 2H), 3.89 (t, *J* = 5.6 Hz, 2H), 3.63 (t, *J* = 5.6 Hz, 2H), 3.13 (s, 3H).

1.3. Synthesis of 5-bromothieno[3,2-b]thiophene-2-carbaldehyde (2)(2)

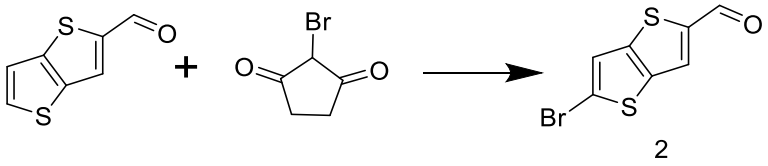

2

A solution of thieno[3,2-b]thiophene-2-carbaldehyde (0.1 g, 0.6 mmol) in dry dimethyl formamide (DMF) (6 mL), then, N-bromosuccinimide (NBS) (0.16 mg, 0.6 mmol) in DMF (6 mL) were added slowly dropwise to the solution and stirred for 2 h at 37 °C. The reaction mixture was diluted with water and filtered off to afford compound **2** (yield 60%). ^{1}H NMR (400 MHz, CDCl3) δ 9.97 (s, 1H), 7.84 (s, 1H), 7.35 (s, 1H).

1.4. Synthesis of 5-((2-hydroxyethyl)(methyl)amino)thieno[3,2-b]thiophene-2-carbaldehyde (3)(1)

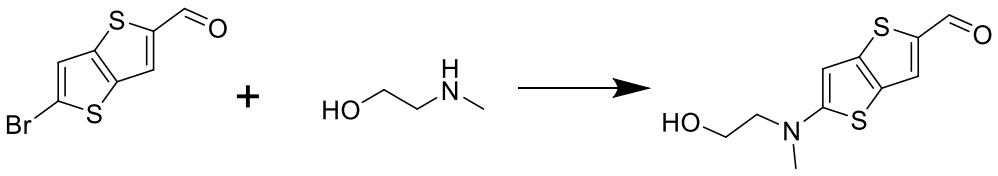

3

Compound **2** (0.1 g, 0.4 mmol), CuI (0.015 mg, 0.08 mmol), K_3PO_4 (0.254 g, 1.2 mmol) and (L)-proline (0.184 g, 0.16 mmol) were added in 3 mL N-methylaminoethanol, and the resulting mixture was stirred 10 h at 90 ℃. After allowing the reaction to cool to room temperature, the mixture was diluted with 50 mL of water, extracted with DCM,

and dried over Na_2SO_4. The crude product was purified by silica gel column chromatography (PE: EA = 1:1, v/v) to yield compound **3** (yield 50%). ^{1}H NMR (400 MHz, DMSO-d6) δ 9.66 (s, 1H), 8.05 (s, 1H), 6.30 (s, 1H), 4.86 (t, J = 5.5 Hz, 1H), 3.64 (q, J = 5.7 Hz, 2H), 3.44 (d, J = 5.7 Hz, 2H), 3.07 (s, 3H).

1.5. Synthesis of (Z)-4-(1-cyano-2-(5-((2-hydroxyethyl)(methyl)amino)thieno[3,2-b]thiophen-2-yl)vinyl)benzonitrile (HBC620)(1)

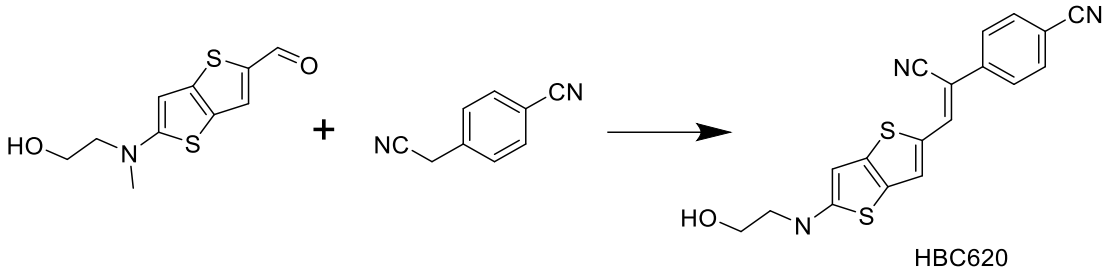

Compound **3** (0.1 g, 0.41 mmol) and 4-cyano-benzeneacetonitrile (0.013g, 0.09 mmol) in 2 mL dry methanol, and two drops of piperidine were added and stirred at room temperature for 1 h. After allowing the reaction to cool to room temperature, the crude product was purified by silica gel column chromatography (CH_2Cl_2: Triethylamin = 100:1, v/v) to yield compound HBC620 (yield 13%). ^{1}H NMR (400 MHz, DMSO-d6) δ 8.37 (s, 1H), 7.88 (d, J = 8.5 Hz, 2H), 7.84 (s, 1H), 7.79 (d, J = 8.5 Hz, 2H), 6.35 (s, 1H), 4.91 - 4.85 (t, 1H), 3.65 (q, J = 5.5 Hz, 2H), 3.45 (t, J = 5.6 Hz, 2H), 3.33 (s, 1H), 3.09 (s, 3H).

1.6. Synthesis of ((Z)-2,6-difluoro-4-((2-methyl-5-oxooxazol-4(5H)-ylidene)methyl)phenyl acetate (4)(3)

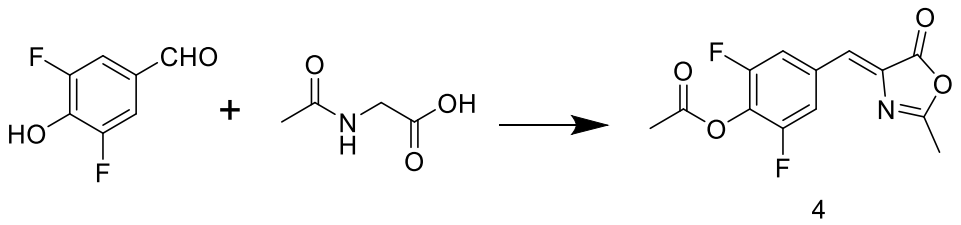

4

3,5-difluoro-4-hydroxybenzaldehyde (1.25 g，7.9 mmol), N-Acetylglycine (0.925 g, 7.90 mmol), anhydrous sodium acetate (0.650 g, 7.92 mmol) were added in 25 mL acetic anhydride, and the mixture was stirred 4 h at 120 ℃. After allowing the reaction to cool to room temperature, cold ethanol (30 ml) was added, and the reaction was placed at 4 ℃ through the night. The crude product was washed with ice ethanol and hot water. Then, it was dried to afford yellow solid compound **4** (0.7 g, yield 32%). ^{1}H NMR (400 MHz, CDCl3) δ 8.04 (d, J = 9.0 Hz, 2H), 7.12 (s, 1H), 2.45 (s, 3H), 2.43 (s, 3H).

1.7. Synthesis of (Z)-4-(3,5-difluoro-4-hydroxybenzylidene)-2-methyl-1-(2,2,2-trifluoroethyl)-1H-imidazol-5(4H)-one (DFHBI-1T)(3)

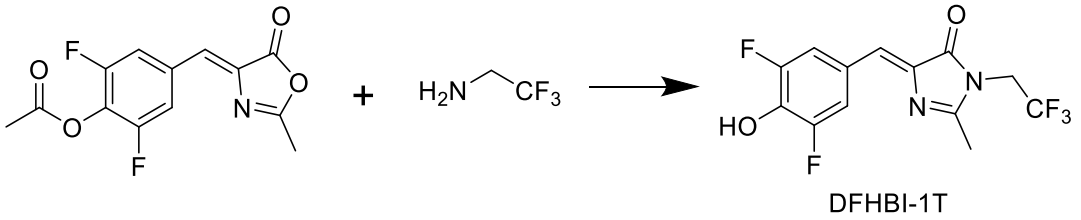

DFHBI-1T

Compound **4** (0.2 g, 0.71 mmol), 2,2,2-Trifluoroethylamine (0.11 g, 1.065 mmol), and potassium carbonate (0.15 g, 1.1 mmol) were added in 1.7 mL absolute ethanol, and the mixture was refluxed for 5 h. After allowing the reaction to cool to room temperature, the solvent was removed under reduced pressure and the reaction and mixture were redissolved in a mixture of ethyl acetate and 500 mM sodium acetate pH 3.0. The organic layer is extracted and dried over Na_2SO_4. The crude product was purified by silica gel column chromatography (CH_2Cl_2: EtOH = 10:1) to yield compound DFHBI-1T (yield 25%). ^{1}H NMR (400 MHz, DMSO-d6) δ 11.05 (s, 1H), 7.99 (d, J = 8.7 Hz, 2H), 7.04 (s, 1H), 4.57 (q, J = 9.3 Hz, 2H), 2.42 (s, 3H).

2. Experimental Section

2.1. Materials and Instruments

Materials

All the organic reagents were purchased from commercial suppliers (Bide Pharmatech or Energy Chemical) and used without further purification unless otherwise stated. Extra dry solvents were purchased from Energy Chemical (Shanghai, China). Magnesium chloride ($MgCl_2$), magnesium sulfate anhydrous ($MgSO_4$), potassium chloride (KCl), dithiothreitol (DTT), urea, diethylpyrocarbonate (DEPC)-treated water, tris(hydroxymethyl)aminomethane (Tris), tetrasodium salt (EDTA), N-[2-Hydroxyethyl] piperazine-N'-[2-ethanesulfonic acid sodium salt (HEPES), Poly-D-lysine Solution were purchased from Sinopharm Chemical Reagent Co., Ltd (Shanghai, China). Spermidine and glycogen were purchased from Adamas Life (Shanghai, China). NTP Mix, DNase I, Hoechst 33342 staining solution, Lipo3000 was purchased from Thermo Fisher Scientific (USA). 40% Acr-Bis (39:1) was purchased from Jiangsu KeyGEN BioTECH Co., Ltd (Nanjing, China). 6× DNA loading buffer purchased from TIANGEN (Beijing, China). DNA ladder purchased from Takara Biomedical Technology (Beijing) Co., Ltd. MTS solution purchased from Saint-Bio (Shanghai, China). Dulbecco's modified eagle medium (DMEM), and fetal bovine serum (FBS) were purchased from Invitrogen (Gibco, USA), serum-free cell freeze was purchased from New Cell & Molecular Biotech Com., Ltd. SYBR Green II RNA dye was purchased from Solarbio (Beijing, China). Qubit® RNA BR Assay Kits were purchased from ThermoFisher Scientific (USA). To create and maintain an RNase-free environment, all the solutions containing RNAs were prepared with diethylpyrocarbonate (DEPC)-treated water. All the stock solutions of the synthetic ligands were prepared in DMSO with a concentration of 10 mM and stored at -20 ℃.

Ultrapure water obtained from a Millipore water purification system (≥ 18 MΩ, Milli-Q, Millipore, Billerica, MA) was used in all runs.

Instruments

Thin-layer chromatography analysis was performed on silica gel plates, and column chromatography was conducted by silica gel (mesh 200) columns. ^{1}H NMR spectra were recorded at 400 MHz on a Bruker-400 spectrometer with tetramethylsilane (TMS) as the internal standard. pH value was measured by a pH meter (Mettler-Toledu, Sweden). Fluorescence intensity measurements were recorded on a Photon Technology International (PTI) QM40 fluorescence spectrophotometer (HORIBA) or Synergy^{TM} Mx multi-mode microplate reader (BioTek, USA), and the quartz cuvette with 2 mm× 10 mm path length was used for spectrum measurement. The excitation and emission slit widths were kept at 5 nm with PTI measurements. UV-vis absorption spectra were performed on a UV-vis spectrophotometer (Agilent). Cells imaging was performed on a confocal laser scanning microscope (CLSM) (Nikon, Eclipse TE2000-E, Japan). All the fluorescence images were digitized and analyzed with ImageJ.

2.2. Nucleic Acid Preparation

Oligonucleotides DNA oligonucleotides (purified by PAGE) and RNA oligomers (purified by HPLC) were synthesized from Sangon Biotech (Shanghai, China). Oligonucleotide sequences are provided in Supporting Data Table S1-2. To obtain the full-length DNA template for in vitro transcription of the light-up RNA sensor platform, a 15 bp hybridization was designed between primer 1 (5'-TAA TAC GAC TCA CTA TAG GTC AAC ATC AGT CTG ATA AGC TAT GTT CGC ATA GCT TAT CA-3') and primer 2 (5'-TAT CAC CGA CAC GCC ACG ATT GGG GAT TTC TCC CGG CGC CAG TGT GAT AAG CTA TGC GA-3') for extension using T3 DNA polymerase (TSINGKE). The resulting dsDNA products were precipitated with 75% ethanol and

resuspended in 50 μL diethyl pyrocarbonate (DEPC) water from Sangon Biotech (Shanghai, China).

In vitro transcription of RNA sensor A 100 μL transcription reaction system was prepared for 1× RNA sensor and aptamer by mixing the transcription buffer containing 40 pmol DNA templates, 80 mM HEPES-KOH (pH 7.5), 24 mM $MgCl_2$, 2 mM Spermidine HCl, 40 mM DTT, 2 mM NTP mix, and 50 units of T7 RNA polymerase (lab prepared stock). For 4×, 8× and 16× RNA sensors, the dsDNA templates were the polymerase chain reaction (PCR) from the corresponding plasmids. The reaction system was incubated at 37°C for 3 h and then treated with DNase I (5 U, from Thermo Fisher) for 15 min at 37°C. The RNA sensor was purified by denaturing 10% PAGE. The RNA products were quantified using fluorescence values with Qubit® RNA BR Assay Kits.

2.3. Fluorescent experiments

To determine the responses of the light-up RNA sensor platform, a total volume of 20 μL reaction system containing miRNA-Pepper or New Pepper sensor (1 μM), miR-21 or miR-122 (1 μM) and 5 μM HBC in 40 mM HEPES, 5 mM $MgCl_2$, 100 mM KCl was incubated at 37°C for 30 min, then recorded fluorescence with Photon Technology International (PTI) QM40 fluorescence spectrophotometer (HORIBA) or SynergyTM Mx multi-mode microplate reader (BioTek, USA). To test the response dynamics, a light-up RNA sensor (1 μM) was incubated at 37°C, and the fluorescence was recorded over a continuous 2 h. To determine the response temperature, a light-up RNA sensor (1 μM) was incubated at different temperatures (20°C, 25°C, 37°C, 42°C), and then the fluorescence spectra were recorded. To determine the reaction buffer, a light-up RNA sensor (1 μM) was reacted in Tris-HCl buffer (10 mM Tris-HCl), HEPES buffer (20 mM HEPES), and K_2HPO_4 (50 mM K_2HPO_4) pH 7.5, 5 mM $MgCl_2$, 100 mM KCl, 10 mM NaCl, and the fluorescence intensity was recorded. To determine the limit of

determination, a 1 μM RNA sensor was incubated with different concentrations of target miRNA (0, 1, 3, 5, 7, 10, 30, 50, 70, and 100 nM).

To study the selectivity of the RNA sensor platform, different substances, including miR-21, miR-122, miR-224, iRFP mRNA, mCherry, and LO2 cell lysates, were incubated with 1 μM light-up RNA sensor in the optimal reaction condition. About 10^4 LO2 Cells were digested with trypsin and washed with PBS, then treated with 200 μL of radioimmunoprecipitation assay (RIPA) buffer (purchased from Beyotime) and centrifuged at 12000 rpm at 4°C for 5 min, collect the supernatant.

To demonstrate the feasibility of constructing an orthogonal dual-color platform, a total volume of 100 μL reaction system containing NP mi21LS (0.5 μM), Sq mi21LS(0.5 μM), miR-21 (1 μM) and 5 μM HBC620 ((4-((2-hydroxyethyl) (methyl)amino)-benzylidene)-cyanophenyl-acetonitrile), 5 μM DFHBI-1T ((Z)-4-(3,5-difluoro-4-hydroxybenzyl-dene)-2-methyl-1-(2,2,2-trifluoroethyl)-1H-imidazol-5(4H)-one) in 40 mM HEPES, 5 mM $MgCl_2$, 100 mM KCl was incubated at 37°C for 30 min, then recorded fluorescence in 450 nm and 577 nm excitation with PTI spectrofluorometer.

To determine the differentiation ability of the RNA sensor platform for target miRNA, a 100 μL reaction system containing miR-122-Pepper sensor (0.5 μM), miR-21-Squash sensor, 5 μM HBC620 and 5 μM DFHBI-1T, then miR-21 (0.5 μM) or miR-122 (0.5 μM) was incubated separately, and the fluorescence was recorded at 450 nm and 577 nm excitation with a PTI.

2.4. Gel electrophoresis analysis

To determine the design strategy of the RNA sensor, about 300 ng of the fluorescence RNA aptamer, modified RNA aptamer, and the reaction product containing RNA sensor and target miRNA were loaded into a well of precast 10 % TBE PAGE gel and run at

110 V for 1 h in 1× TBE buffer. After electrophoresis, the gel was stained for 10 min with 2 μM HBC or DFHBI-1T in the corresponding imaging buffer. The gel was imaged using Azure biosystems 300Q with 472±15 nm excitation and 513 nm emission for HBC530 and DFHBI-1T, 524±12 nm excitation, and 595 nm emission for HBC620. Next, the gel was washed three times for 5 min with water, then stained for 15 min with SYBR Green II and imaged under the SYBR channel (302 nm excitation and 590 nm emission).

In vitro characterization of tandem arrays of light-up RNA sensor. To study the tandem arrays of the RNA sensor, 200 nM tandem arrays of RNA sensor (1×, 4×, 8× and 16×) and the arrays RNA sensor of different linker were incubated with target miRNA in the imaging buffer described above, containing 5 μM HBC. The 8× RNA sensor with or without target miRNA samples was analyzed using 1% agarose gel electrophoresis at 110 V for 1 h in 1× TBE buffer, and the gel was pre-stained with 1× GeneGreen (TSINGKE).

2.5. UV-vis analysis

100 μL solution containing HBC530 (5 μM) with or without annealed New Pepper (10 μM) in the reaction buffer (40 mM HEPES, 5 mM $MgCl_2$, 100 mM KCl) was incubated at 37 °C for 10 min. The UV-Vis spectra for each sample were recorded in a UV-vis spectrophotometer.

2.6. Total RNA extraction and qRT-PCR analysis of miRNA in cells

Total RNA was isolated from Huh7, LO2, MCF-7, A549, and HEK293T cells using RNAprep pure Cell/Bacteria Kit (Tiangen Biotech Co., Ltd. (Beijing) following the manufacturer's protocol.

To analyze the expression of miRNA, total RNA (1 μg) was transcribed into

complementary DNA (cDNA) using the miRNA RT-primer with 5 pmol RT-primer using Evo M-MLV RT Mix Kit (reverse transcriptase, Accurate biology, Changsha) on an S1000^{TM} Thermal Cycler (Bio-Rad Laboratories, Inc., USA) according to the manufacturer's instructions. PCR was performed with SYBR® Green Premix Pro Tag HS Qpcr Kit (Accurate biology, Changsha) on a QuantStudio 7 Flex (Invitrogen Life Technologies, Carlsbad, California, USA). The 20 μL of solution contains 2 μL of cDNA sample, 0.4 μL of forward primer (10 μM), 0.4 μL of reverse primer (10 μM), 10 μL of 2×SYBR® Green Pro Tag HS Premix, and 7.2 μL of RNase free water. The PCR was performed in the following conditions: 95˚C for 30 s, 40 cycles of 95˚C for 5 s and 60˚C for 30 s.

2.7. Theoretical Calculation

To explore the fluorescence properties of HBC530, HBC620, DFHBI-1T in water, density functional theory (DFT) was performed using Gaussian 09. The density functional theory calculation with the CAM-B3LYP method was applied to the geometry optimization of all molecules in the ground (S0) and excited state (S1) with a 6-31+G(d) basis set in water. The HOMO and LUMO energies at S0 and S1 states are calculated from the geometrically optimized molecule.

2.8. Molecular docking

To demonstrate the specific recognition of HBC for New Pepper RNA aptamer, molecular docking studies were made by the Autodock Vina(4). The RNA 3D structures were modeled with the public web page of Xiao Lab (http://biophy.hust.edu.cn/new/3dRNA). The structure of HBC is obtained from RCSB Protein Data Bank (PDB: 7EOH). Docking of HBC with New Pepper was performed by AutoDock Vina, and then molecular interactions between them were studied by docking simulations via AutoDock Vina, PyMOL 2.3 software was used to display the

docking model.

2.9. Cell culture and Laser Scanning Confocal Fluorescence Imaging

All cells were cultured with high glucose DMEM containing 10% FBS, 100 U/mL penicillin and 100 μg/mL streptomycin in an incubator (Thermo Scientific) at 37°C under an atmosphere of 5 % CO_2 and 90 % relative humidity.

For imaging experiments, 2.5× 10^4 Huh7, MCF-7, LO2, and HEK293T cells were seeded in a 35 mm confocal dish (Cellvis, Mountainview, CA) and cultured in 1 mL DMEM medium containing 10% FBS, 100 U/mL penicillin and 100 μg/mL streptomycin in an incubator (Thermo Scientific) at 37°C under an atmosphere of 5% CO_2 overnight. Then, the fluorogenic RNA aptamer sensor activated miRNA imaging by transfecting the cell with 500 nM Pepper miRNA sensor, Squash miRNA sensor, or RNA sensor orthogonal platform by Lipo3000 (Thermo Fisher) under standard cell culture condition for at least 6 h. After transfection, the cells were washed three times with PBS. Next, 100 μL PBS, 1× Hoechst 33342, and 2.5 μM DFHBI-1T or HBC620 were added to the cells for 30 minutes (DMSO＜1%). The cells were then washed three times with phenol red-free media buffer. All images were scanned with a confocal laser scanning microscope (CLSM, Nikon A1 plus, Japan) with a 60× objective. Hoechst 33342 with 405 nm excitation, DFHBI-1T with 488 nm excitation, and HBC620 with 561 nm excitation, respectively. Images were further analyzed and quantified by the ImageJ software.

2.10. Cell cytotoxicity determination

1.5× 10^6 HEK293T cells were seeded on 96-well cell culture plates at 37°C with 5% CO_2 and incubated for 12 h. The medium was replaced with a 100 μL medium containing different concentrations of HBC530, HBC620, and DFHBI-1T (DMSO <

1%) for 0.5 h. After washing with PBS, cells were incubated with 10 μL MTS reagent in 100 μL medium at 37°C for 1 h. The absorbance (abs.) of the solution at 490 nm (OD_{490}) was measured in a microplate reader. Cell viability (%) was calculated according to Equation S1. Each experiment was tested with three replicates.

$$Cell\ viability = \frac{[OD_{Sample} - OD_{blank}]}{[OD_{control} - OD_{blank}]} \times 100\% \quad \text{S1}$$

3. Supplemental Tables and Figures

3.1. Supplemental Tables

Table S1. Sequences RNA applied in this study.

Name	Sequence (5' - 3')
Pepper	UCC CCA AUC GUG GCG UGU CGG CCU GCU UCG GCA GGC ACU GGC GCC GGG A
Pepper stem-loop	CCA AUC GUG GCG UGU CGG CCU GCU UCG GCA GGC ACU GGC GCC G
Pepper stem-loop 1	CCA AUC GUG GCG UGU CGG GGC ACG AAA GUG CCC ACU GGC GCC G
Pepper stem-loop 2	CCA AUC GUG GCG UGU CGG CAG UCU UCG GAC UGC ACU GGC GCC G
Pepper mismatched stem	CCA AUC GUG GCG UGU CGG CCU GCU UCG GAC UUC ACU GGC GCC G
Cp Pepper	GCA GGC ACU GGC GCC GCC AAU CGU GGC GUG UCG GCC UGC
New Pepper	GCA GGC ACU GGC GCC GGG AGA AAU CCC CAA UCG UGG CGU GUC GGC CUG C
Squash	GGC UAC AAG GUG AGC CCA AUA AUA CGG UUU GGG UUA GGA UAG GAA GUA GAG CCG UAA ACU CUC UAA GCG GUA GUC
Squash stem 1	UGU GAC AAG GUG AGC CCA AUA AUA CGG UUU GGG UUA GGA UAG GAA GUA GAG CCG UAA ACU CUC UAA GCG GUC ACA
Squash stem 2	UAC GAC AAG GUG AGC CCA AUA AUA CGG UUU GGG UUA GGA UAG GAA GUA GAG CCG UAA ACU CUC UAA GCG GUA GUC
Squash mismatched stem	GGC UAC AAG GUG AGC CCA AUA AUA CGG UUU GGG UUA GGA UAG GAA GUA GAG CCG UAA ACU CUC UAA GCG GCC UAC
NP mi21LS-1	UCA ACA UCA GUC UGA UAA GCU AUU CGU AGC UUA UCA CAC UGG CGC CGG GAG AAA UCC CCA AUC GUG GCG UGU CGG UGA UAA GC
NP mi21LS-2	UCA ACA UCA GUC UGA UAA GCU AUG UUC GCA UAG CUU AUC ACA CUG GCG CCG GGA GAA AUC CCC AAU CGU GGC GUG UCG GUG AUA

NP mi21LS-3	UCA ACA UCA GUC UGA UAA GCU AUG UUC GCA UAG CUU AUC ACU GGC GCC GGG AGA AAU CCC CAA UCG UGG CGU GUC GGA UAA G
FAM-NP mi21LS-3	UCA ACA UCA GUC UGA UAA GCU AUG UUC GCA UAG CUU AUC ACU GGC GCC GGG AGA AAU CCC CAA UCG UGG CGU GUC GGA UAA G-FAM
NP mi21LS-4	UCA ACA UCA GUC UGA UAA GCU AUG GAA ACA UAG CUU AUC ACA CUG GCG CCG GGA GAA AUC CCC AAU CGU GGC GUG UCG GUG AUA
Pepper mi21LS	UCA ACA UCA GUC UGA UAA GCU AUG UUC GCA UAG CUU AUC CAA UCG UGG CGU GUC GGC CUG CUU CGG CAG GCA CUG GCG CCG AUA AG
NP mi122LS-1	CAA ACA CCA UUG UCA CAC UCC AGU UCG CUG GAG UGU GAC ACA CUG GCG CCG GGA GAA AUC CCC AAU CGU GGC GUG UCG GUG UCA
NP mi122LS-2	CAA ACA CCA UUG UCA CAC UCC AGG AAA CUG GAG UGU GAC ACU GGC GCC GGG AGA AAU CCC CAA UCG UGG CGU GUC GGU CAC A
NP mi122LS-3	CAA ACA CCA UUG UCA CAC UCC AGG AAA CUG GAG UGU GAC ACA CUG GCG CCG GGA GAA AUC CCC AAU CGU GGC GUG UCG GUG UCA
NP mi122LS-4	CAA ACA CCA UUG UCA CAC UCC AUG GAA ACA UGG AGU GUC ACU GGC GCC GGG AGA AAU CCC CAA UCG UGG CGU GUC GGU GUC A
Sq mi21LS	UCA ACA UCA GUC UGA UAA GCU AGG AAA CUA GCU UAU CAG ACA AGG UGA GCC CAA UAA UAC GGU UUG GGU UAG GAU AGG AAG UAG AGC CGU AAA CUC UCU AAG CGG UCU GAU
miR-21	UAG CUU AUC AGA CUG AUG UUG A
miR-122	UGG AGU GUG ACA AUG GUG UUU G
miR-224	UCA AGU CAC UAG UGG UUC CGU UUA G
anti-miR-21	UCA ACA UCA GUC UGA UAA GCU A
anti-miR-122	CAA ACA CCA UUG UCA CAC UCC A
iRFP mRNA	CUC CUA UCA CUG UAG GUU UCA CCA UGC G
4× NP mi21LS-1 nt	UCA ACA UCA GUC UGA UAA GCU AUG UUC GCA UAG CUU AUC ACU GGC GCC GGG AGA AAU CCC CAA UCG UGG CGU GUC GGA UAA GaU CAA CAU CAG UCU GAU AAG CUA UGU UCG CAU AGC UUA UCA CUG GCG CCG GGA GAA AUC CCC AAU CGU GGC GUG UCG GAU AAG aUC ACA UCA GUC UGA UAA GCU AUG UUC GCA UAG CUU AUC ACU GGC GCC GGG AGA AAU CCC CAA UCG UGG CGU GUC GGA UAA GaU CAA CAU CAG UCU GAU AAG CUA UGU UCG CAU AGC UUA UCA CUG GCG CCG GGA GAA AUC CCC AAU CGU GGC GUG UCG GAU AAG

4× NP mi21LS-3 nt	UCA ACA UCA GUC UGA UAA GCU AUG UUC GCA UAG CUU AUC ACU GGC GCC GGG AGA AAU CCC CAA UCG UGG CGU GUC GGA UAA Gaa aUC AAC AUC AGU CUG AUA AGC UAU GUU CGC AUA GCU UAU CAC UGG CGC CGG GAG AAA UCC CCA AUC GUG GCG UGU CGG AUA AGa aaU ACA UCA GUC UGA UAA GCU AUG UUC GCA UAG CUU AUC ACU GGC GCC GGG AGA AAU CCC CAA UCG UGG CGU GUC GGA UAA Gaa aUC AAC AUC AGU CUG AUA AGC UAU GUU CGC AUA GCU UAU CAC UGG CGC CGG GAG AAA UCC CCA AUC GUG GCG UGU CGG AUA AG
4× NP mi21LS-5 nt	UCA ACA UCA GUC UGA UAA GCU AUG UUC GCA UAG CUU AUC ACU GGC GCC GGG AGA AAU CCC CAA UCG UGG CGU GUC GGA UAA Gua aau UCA ACA UCA GUC UGA UAA GCU AUG UUC GCA UAG CUU AUC ACU GGC GCC GGG AGA AAU CCC CAA UCG UGG CGU GUC GGA UAA Gua aau UCA ACA UCA GUC UGA UAA GCU AUG UUC GCA UAG CUU AUC ACU GGC GCC GGG AGA AAU CCC CAA UCG UGG CGU GUC GGA UAA Gua aau UCA ACA UCA GUC UGA UAA GCU AUG UUC GCA UAG CUU AUC ACU GGC GCC GGG AGA AAU CCC CAA UCG UGG CGU GUC GGA UAA G
4× NP mi21LS-8 nt	UCA ACA UCA GUC UGA UAA GCU AUG UUC GCA UAG CUU AUC ACU GGC GCC GGG AGA AAU CCC CAA UCG UGG CGU GUC GGA UAA Gaa auu aaa UCA ACA UCA GUC UGA UAA GCU AUG UUC GCA UAG CUU AUC ACU GGC GCC GGG AGA AAU CCC CAA UCG UGG CGU GUC GGA UAA Gaa auu aaa UCA ACA UCA GUC UGA UAA GCU AUG UUC GCA UAG CUU AUC ACU GGC GCC GGG AGA AAU CCC CAA UCG UGG CGU GUC GGA UAA Gaa auu aaa UCA ACA UCA GUC UGA UAA GCU AUG UUC GCA UAG CUU AUC ACU GGC GCC GGG AGA AAU CCC CAA UCG UGG CGU GUC GGA UAA G
4× NP mi21LS-AUUUA	UCA ACA UCA GUC UGA UAA GCU AUG UUC GCA UAG CUU AUC ACU GGC GCC GGG AGA AAU CCC CAA UCG UGG CGU GUC GGA UAA Gau uua UCA ACA UCA GUC UGA UAA GCU AUG UUC GCA UAG CUU AUC ACU GGC GCC GGG AGA AAU CCC CAA UCG UGG CGU GUC GGA UAA Gau uua UCA ACA UCA GUC UGA UAA GCU AUG UUC GCA UAG CUU AUC ACU GGC GCC GGG AGA AAU CCC CAA UCG UGG CGU GUC GGA UAA Gau uua UCA ACA UCA GUC UGA UAA GCU AUG UUC GCA UAG CUU AUC ACU GGC GCC GGG AGA AAU CCC CAA UCG UGG CGU GUC GGA UAA G
4× NP mi21LS-AAAAA	UCA ACA UCA GUC UGA UAA GCU AUG UUC GCA UAG CUU AUC ACU GGC GCC GGG AGA AAU CCC CAA UCG UGG CGU GUC GGA UAA Gaa aaa UCA ACA UCA GUC UGA UAA GCU AUG UUC GCA UAG CUU AUC ACU GGC GCC GGG AGA AAU CCC CAA UCG UGG CGU GUC GGA UAA Gaa aaa UCA ACA UCA GUC UGA UAA GCU AUG UUC GCA UAG CUU AUC ACU GGC GCC GGG AGA AAU CCC CAA UCG UGG CGU GUC GGA UAA Gaa aaa UCA ACA UCA GUC UGA UAA GCU AUG UUC GCA UAG CUU AUC ACU GGC GCC GGG AGA AAU CCC CAA UCG UGG CGU GUC GGA UAA G

4× NP mi21LS-GGGG	UCA ACA UCA GUC UGA UAA GCU AUG UUC GCA UAG CUU AUC ACU GGC GCC GGG AGA AAU CCC CAA UCG UGG CGU GUC GGA UAA Ggg ggg UCA ACA UCA GUC UGA UAA GCU AUG UUC GCA UAG CUU AUC ACU GGC GCC GGG AGA AAU CCC CAA UCG UGG CGU GUC GGA UAA Ggg ggg UCA ACA UCA GUC UGA UAA GCU AUG UUC GCA UAG CUU AUC ACU GGC GCC GGG AGA AAU CCC CAA UCG UGG CGU GUC GGA UAA Ggg ggg UCA ACA UCA GUC UGA UAA GCU AUG UUC GCA UAG CUU AUC ACU GGC GCC GGG AGA AAU CCC CAA UCG UGG CGU GUC GGA UAA G
8× NP mi21LS	UCA ACA UCA GUC UGA UAA GCU AUG UUC GCA UAG CUU AUC ACU GGC GCC GGG AGA AAU CCC CAA UCG UGG CGU GUC GGA UAA Gua aau UCA ACA UCA GUC UGA UAA GCU AUG UUC GCA UAG CUU AUC ACU GGC GCC GGG AGA AAU CCC CAA UCG UGG CGU GUC GGA UAA Gua aau UCA ACA UCA GUC UGA UAA GCU AUG UUC GCA UAG CUU AUC ACU GGC GCC GGG AGA AAU CCC CAA UCG UGG CGU GUC GGA UAA Gua aau UCA ACA UCA GUC UGA UAA GCU AUG UUC GCA UAG CUU AUC ACU GGC GCC GGG AGA AAU CCC CAA UCG UGG CGU GUC GGA UAA Gua aau UCA ACA UCA GUC UGA UAA GCU AUG UUC GCA UAG CUU AUC ACU GGC GCC GGG AGA AAU CCC CAA UCG UGG CGU GUC GGA UAA Gua aau UCA ACA UCA GUC UGA UAA GCU AUG UUC GCA UAG CUU AUC ACU GGC GCC GGG AGA AAU CCC CAA UCG UGG CGU GUC GGA UAA Gua aau UCA ACA UCA GUC UGA UAA GCU AUG UUC GCA UAG CUU AUC ACU GGC GCC GGG AGA AAU CCC CAA UCG UGG CGU GUC GGA UAA Gua aau UCA ACA UCA GUC UGA UAA GCU AUG UUC GCA UAG CUU AUC ACU GGC GCC GGG AGA AAU CCC CAA UCG UGG CGU GUC GGA UAA G
16× NP mi21LS	8× NP mi21LS-uaaau-8× NP mi21LS

Green bases indicated the corn sequences for Pepper or Squash. Orange bases indicated the stem sequences for Pepper or Squash. Underlined medium turquoise bases indicated the sequences complementary to miR-21 or miR-122. Bases in lower cyan cases were linkers.

Table S2. Sequences of the primer sequences in qRT-PCR.

Name	Sequence (5' - 3')
RT-primer for miR-21	GTC GTA TCC AGT GCA GGG TCC GAG GTA TTC GCA CTG GAT ACG ACT CAA CA
Forward primer for miR-21	GCC CGC TAG CTT ATC AGA CTG ATG
Reverse primer for miR-21	GTG CAG GGT CCG AGG T
RT-primer for miR-122	GTC GTA TCC AGT GCA GGG TCC GAG GTA TTC GCA CTG GAT ACG ACC AAA CAC
Forward primer for miR-122	GCC GTG GAG TGT GAC AAT GGT

Reverse primer for miR-122	GTG CAG GGT CCG AGG T
Forward primer for GAPDH	CAA CTC ACT CAA GAT TGT CAG CAA
Reverse primer for GAPDH	GGG ATG GAC TGT GGT CAT GA

Table S3. The detection performance of previously reported genetically encoded sensors for microRNA detection.

Name	Mode	Fluorogenic RNA aptamers	Target	Activation fold	LOD
FASTmiR(5)	Single color	Spinach	miR-171, miR-122	N/A	N/A
Pandan(6)	Single color	Spinach 2	dme-bantam-5p, has-miR-21-5p, has-let7f, has-miR-375	~4-~100	N/A
RNA Sensor(7)	Ratiometric	GFP/SRB2	miR-21	~8	0.3 nM
dual-color light-up RNA sensor(8)	Ratiometric	Mango/SRB2	miR-224	~5	N/A
iLAMP(9)	Ratiometric	Mango/SRB2	miR-155, miR-21	~8	0.02 nM
miLS (This work)	Orthogonal dual-color	Pepper/Squash	miR-21, miR-122	~16-~44	0.2 nM

N/A: not available. LOD: limit of detection.

3.2. Supplemental Figures

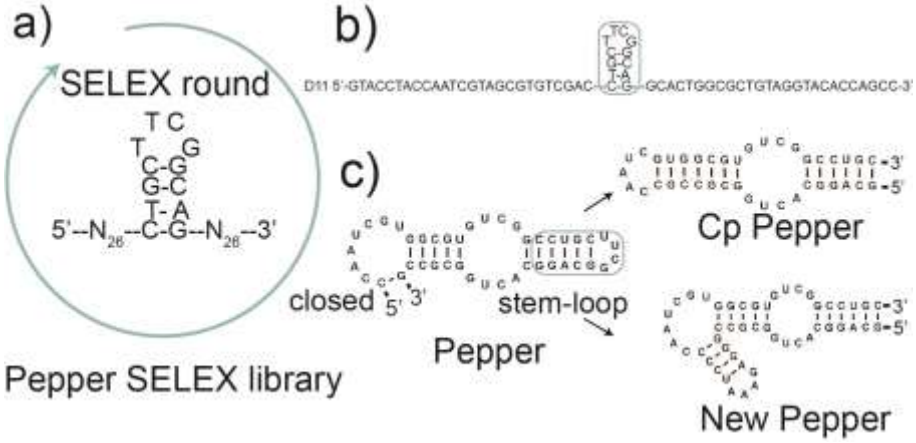

Figure S1. Scheme for the design of a light-up RNA sensor from the screening library as the source. (a) Schematic of Pepper SELEX library using stem-loop as an anchor for screening. (b) The D11 sequence of Pepper after 8 rounds of SELEX. (c) The design of the circularly permuted Pepper.

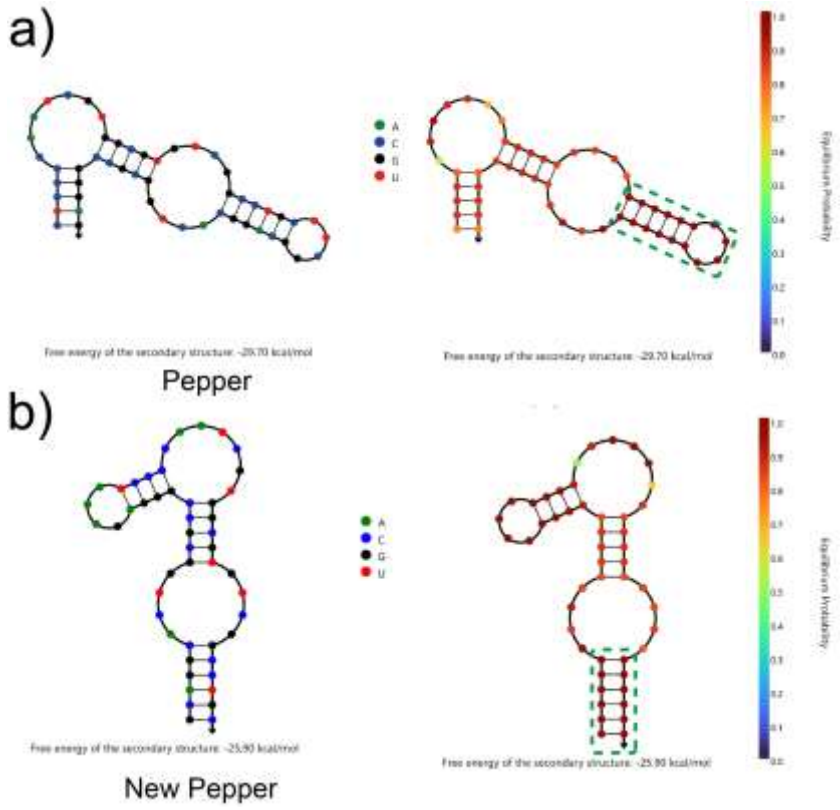

Figure S2 Thermodynamic prediction of the secondary structures of (a) Pepper and (b) New Pepper using the *NUPACK* web.

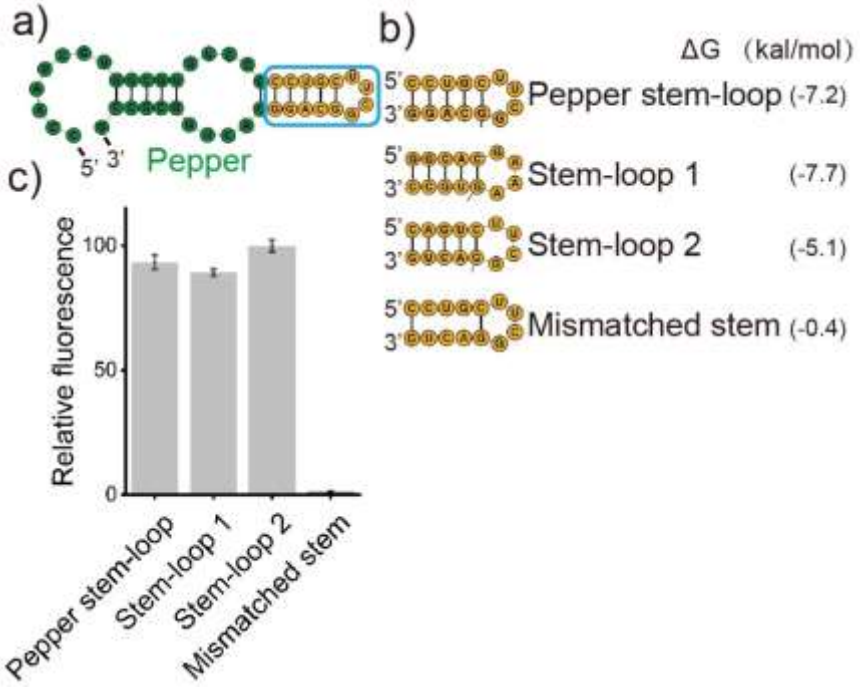

Figure S3. (a) The predicted secondary structure of a minimized Pepper sequence with stem-loops circled by a blue box. The structure was generated using *RNA Structure*. (b) Mutation analysis of stem-loop of Pepper. The stem-loop of Pepper was replaced by either of the three randomly selected stem-loops of difference sequence. The "mismatched stem" retains the original UUCG tetraloop found in Pepper, but replaces the stem with three mismatched nucleotides to prevent duplex formation, ΔG increased. (c) Relative fluorescence of Pepper with different stem-loops. Data was repeated three times. Relative fluorescence is defined as the ratio of the fluorescence value to the maximum fluorescence.

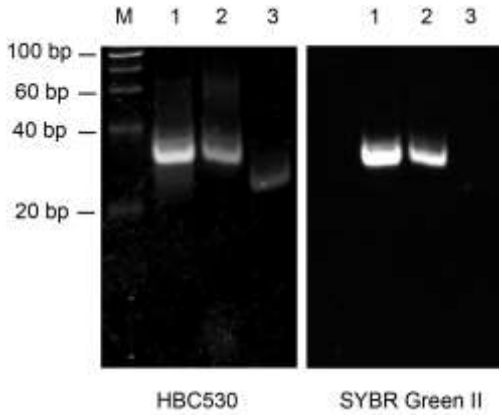

Figure S4. (a) 10% PAGE analysis of the design of the circularly permuted Pepper stained using HBC530 or SYBR Green II. Lane 1, New Pepper; Lane 2, Pepper; Lane 3, Cp Pepper; Lane M denotes molecular weight markers. Gels were stained first with HBC530 (left) and subsequently with SYBR Green II (right).

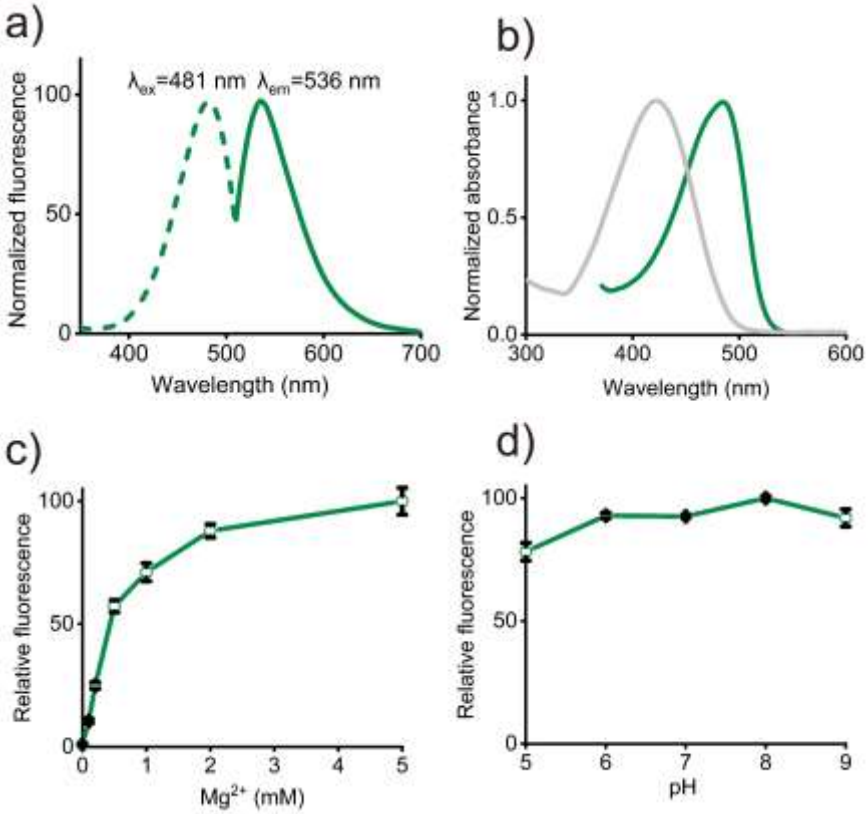

Figure S5. (a) The excitation (Ex) and emission (Em) spectra of New Pepper bound to HBC530. (b) Normalized UV-vis absorbance spectra of New Pepper530 (green) or only HBC (gray). (c) Magnesium dependence of New Peppr. (d) Effect of pH on the fluorescence of New Pepper bound to HBC530. All data represent means ± SD, n=3. Relative fluorescence is defined as the ratio of the fluorescence value to the maximum fluorescence.

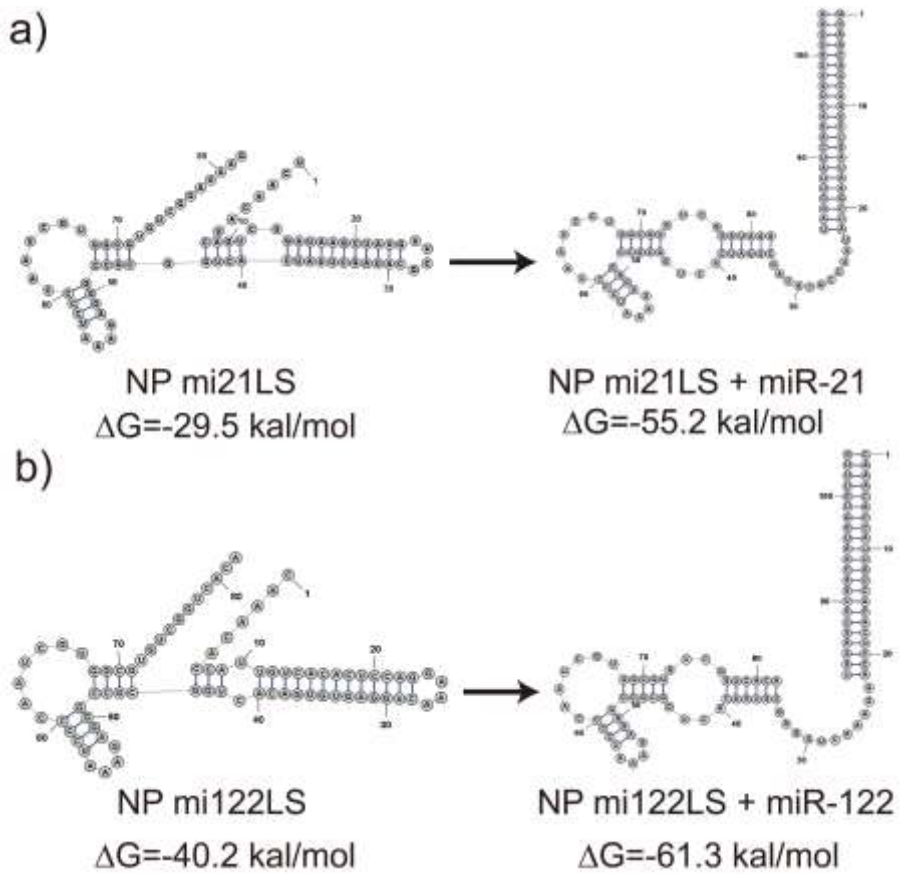

Figure S6. (a) The predicted secondary structure of NP mi21LS and NP mi21LS with the target. (b). The predicted secondary structure of NP mi122LS and NP mi122LS with the target. The structure was generated using *RNA Structure*.

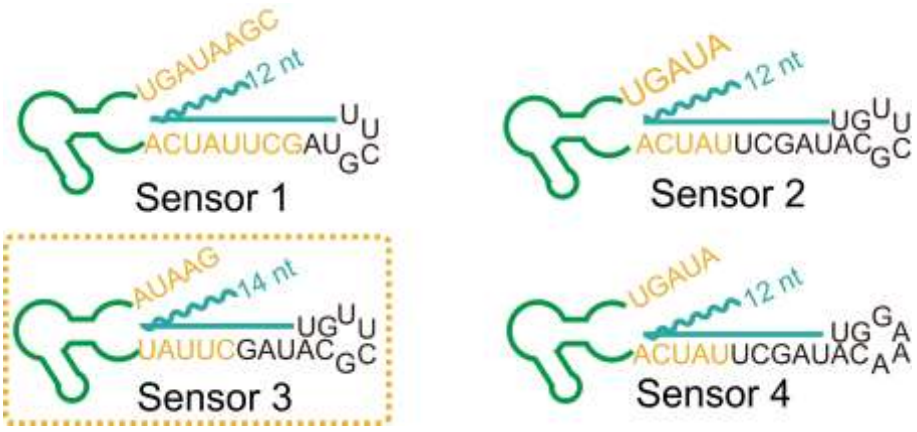

Figure S7. Schematic for the optimization of NP mi21LS, containing the toehold sequence length is denoted by cyan lines, P1 stem sequence is denoted by yellow bases, and tetraloop UUCG or GAAA. In Sensor 1, the free P1 stem length is 8nt, which makes it possible to form a stable stem of pepper P1. In the absence of target RNA, the fluorescent background signal is high. The free P1 stem is reduced to 5nt in sensor 2 to reduce the background. To further improve the signal-to-noise ratio, the toehold length was increased to 14nt in sensor 3. In order to increase sensor stability, tetraloop UUCG was changed to GAAA, but the signal-to-noise ratio was not improved relative to Sensor 2. (Figure 2b).

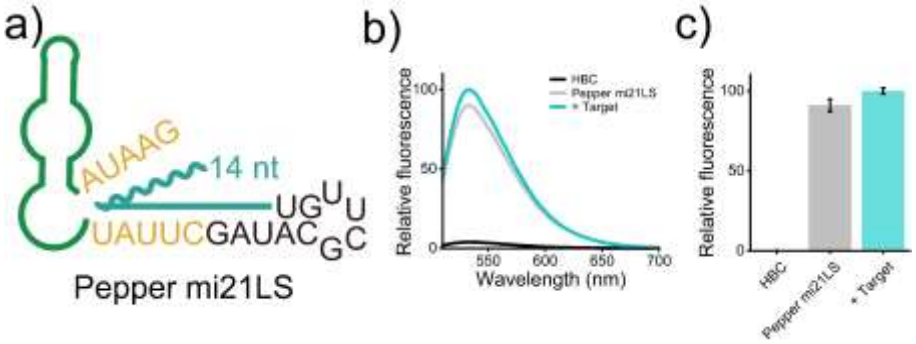

Figure S8 (a) Schematic for the optimization of Pepper mi21LS, using the same sequence design as the NP mi21LS. (b) Fluorescence spectra of HBC530 in the presence of 1 μM Pepper mi21LS and 1 μM Pepper mi21LS with miR-21. (c) Relative fluorescent intensity of Pepper mi21LS with and without target RNA. Error bars are standard deviations in three repetitive assays.

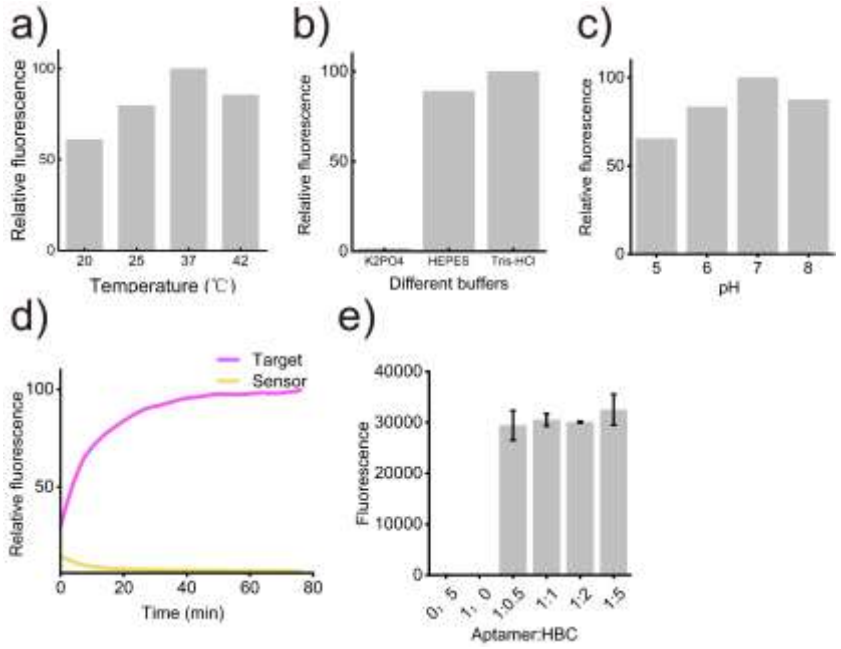

Figure S9. (a) Temperature-dependent fluorescence responses for the NP mi21LS (1 μM) miR-21 (1 μM) in the presence of HBC530. (b). The relative fluorescence for the NP mi21LS (1 μM) miR-21 (1 μM) in the presence of HBC530 incubated in different buffers. (c) pH-dependent fluorescence responses for the NP mi21LS (1 μM) miR-21 (1 μM) in the presence of HBC530. (d) The reaction kinetics analysis for the NP mi21LS (1 μM) miR-21 (1 μM). (e) The relative fluorescence of NP mi21LS with different HBC530. The sample with a ratio of the NP mi21LS to HBC530 of 0:5 was a negative control. Relative fluorescence is defined as the ratio of the fluorescence value to the maximum fluorescence value.

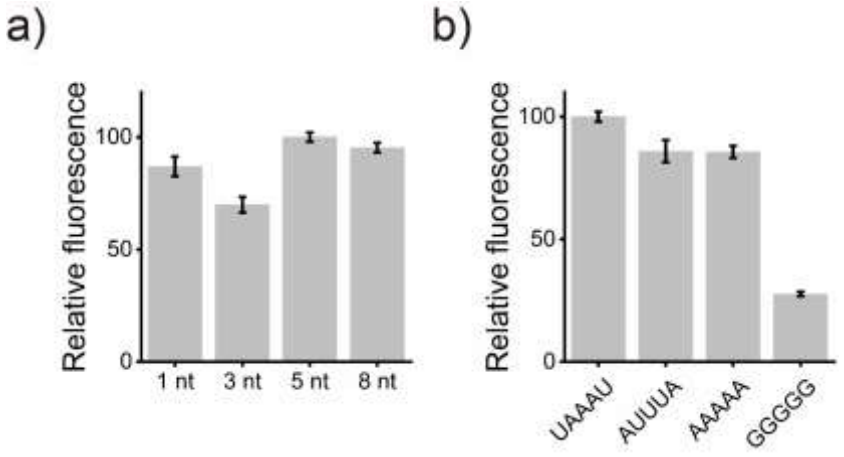

Figure S10 (a) Relative fluorescence of intensity of 4× NP mi21LS with alteration of the length linker between adjacent mi21LS. (b) Relative fluorescence of intensity of 4× NP mi21LS with alteration of the compositions 5nt linker between adjacent mi21LS.

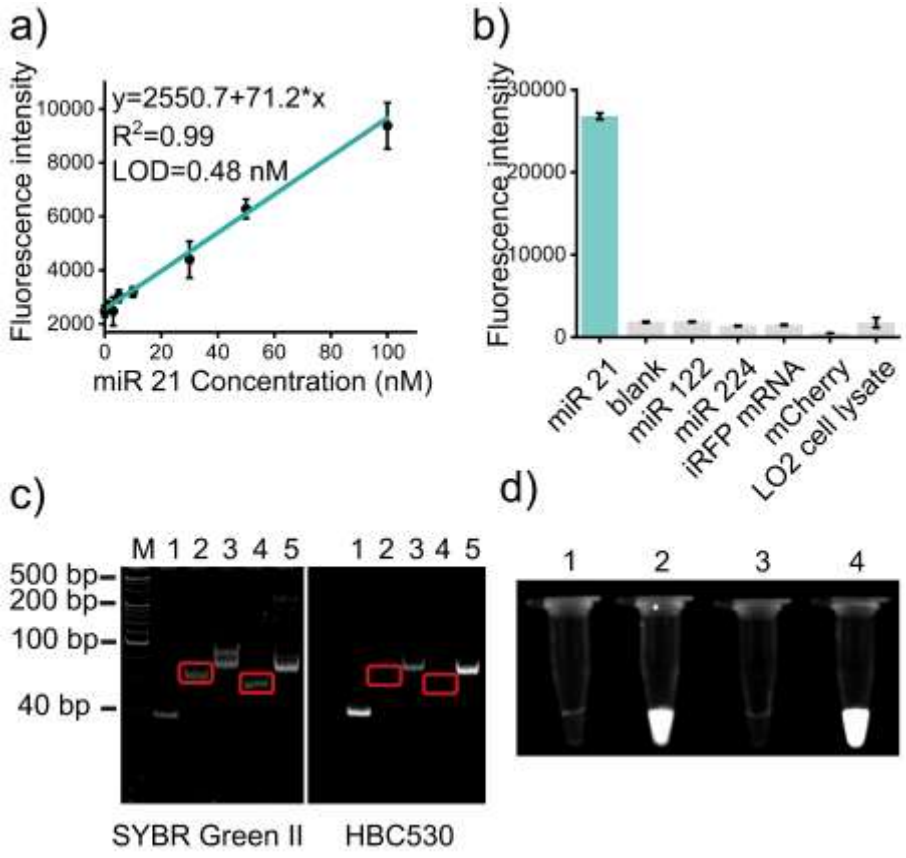

Figure S11. (a) The linear relationship between the fluorescence intensity of NP mi21LS and miR-21 concentrations ranged from 0 to 100 nM. (b) Selectivity study for the NP mi21LS. Fluorescence intensities of miLS at λ_{em}=530 nm to different substances. (c) 10% PAGE analysis of miLS with or without miR-21 stained using HBC530 or SYBR Green II. Lane 1, New Pepper; Lane 2, mi21LS; Lane 3, NP mi21LS with miR-21; Lane 4, NP mi122LS; Lane 5, NP mi122LS with miR-122; M denotes molecular weight markers. Gels were stained first with HBC530 (right) and subsequently with SYBR Green II (left). The bands showing differences in the two gel images are circled in red. (d) The tubes fluorescence imaging for miLS. Lane 1, NP mi21LS; Lane 2, NP mi21LS with miR-21; Lane 3, NP mi122LS; Lane 4, NP mi122LS with miR-122. (λ_{ex}: 472±15 nm, λ_{em} = 513 nm).

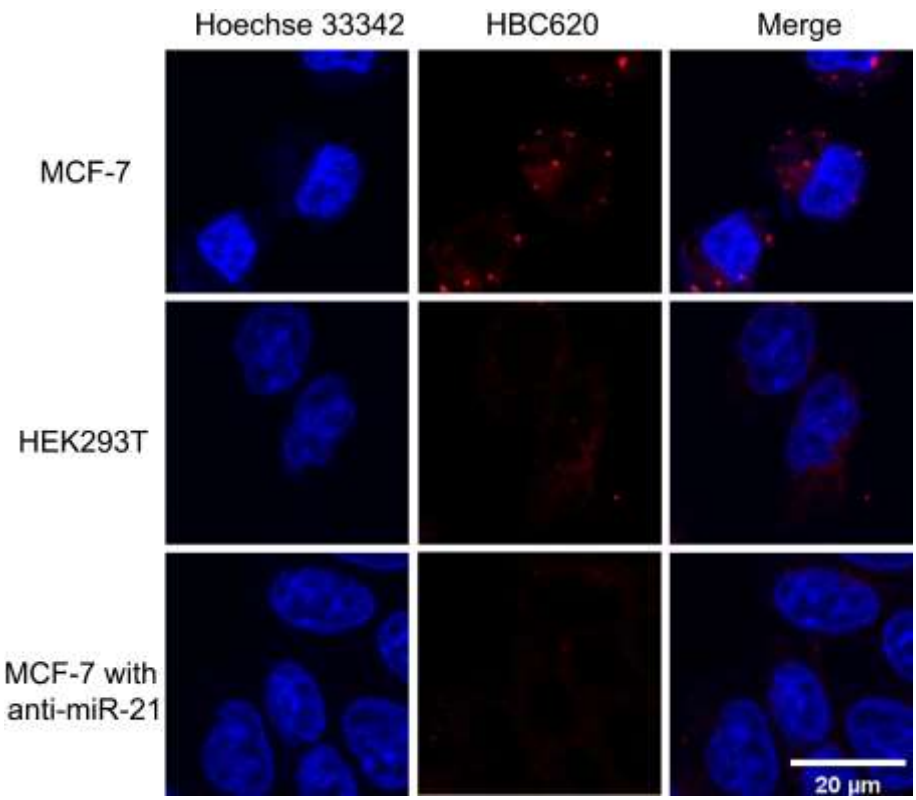

Figure S12. Confocal imaging results of the MCF-7, HEK293T and MCF-7 with anti-miR-21 cell line transfected the fluorogenic NP mi21LS system when incubated with HBC620. Scale bar, 20 μm.

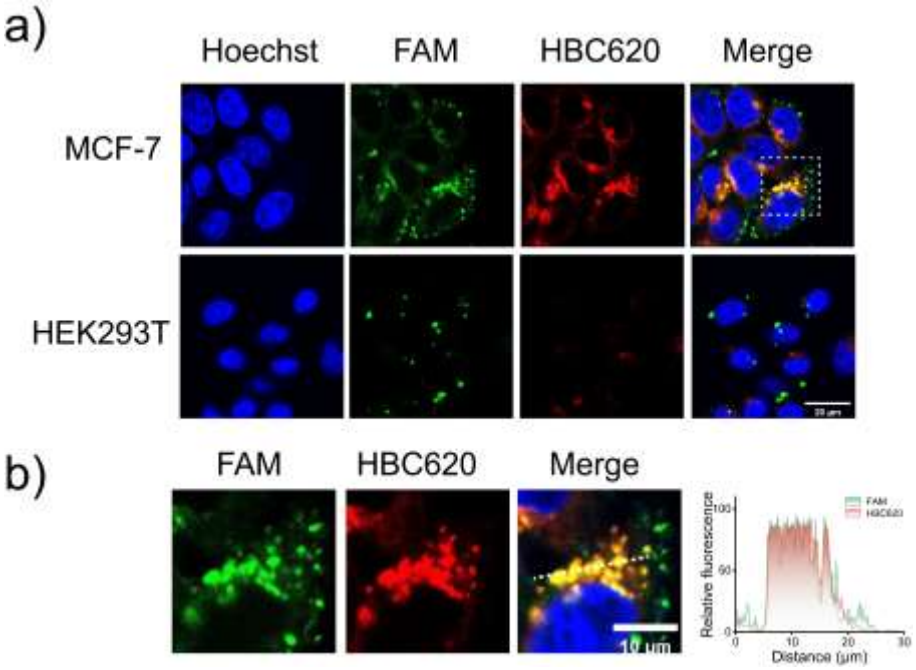

Figure S13 (a) Confocal imaging results of the MCF-7 and HEK293T cell line transfected with FAM-tagged NP mi21LS system when incubated with HBC620. Scale bar, 20 μm. (b) The zoomed-in images of the region denoted by the white boxes of (a). Relative fluorescence intensity profile of regions of interest (white line in left panels). Scale bar, 10 μm

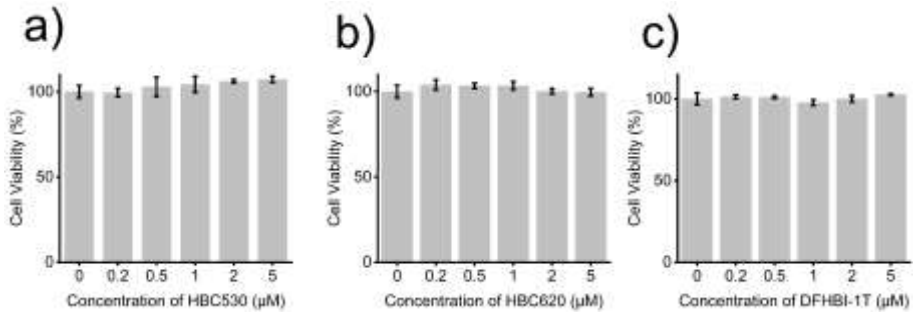

Figure S14. Cytotoxicity assays of HBC530 (a), HBC620 (b) and DFHBI-1T (c) in HEK293T cells. Data represent the mean ± s.d. from three cell cultures. Error bars are standard deviations in three repetitive assays.

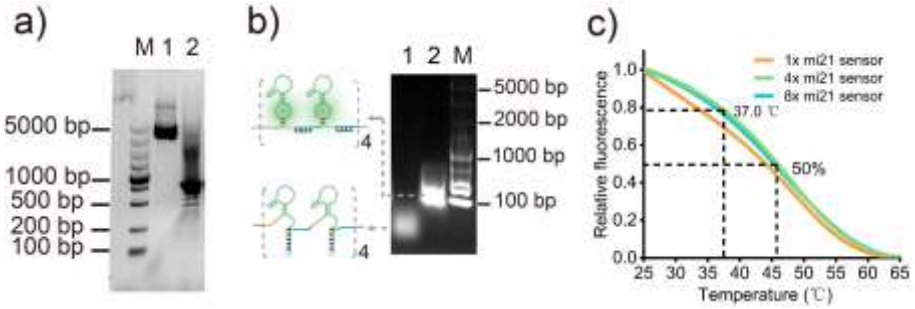

Figure S15. (a) Agarose gel electrophoresis analysis for the 8× NP mi21LS transcriptional template for 1 h, 110 V electrophoresis migration in 0.5× TBE buffer. Especially, Lane M: 5000 bp Marker; Lane 1: pAPU6-8× NP mi21LS plasmid DNA; Lane 2: 8× NP mi21LS transcriptional template from PCR DNA. (b) 1% agarose gel analysis of 8× NP mi21LS with or without miR-21 stained using GeneGreen. (c) Temperature-dependence relative fluorescence intensity of 1×, 4× and 8× NP mi21LS with the target. Relative fluorescence is defined as the ratio of the fluorescence value to the maximum fluorescence.

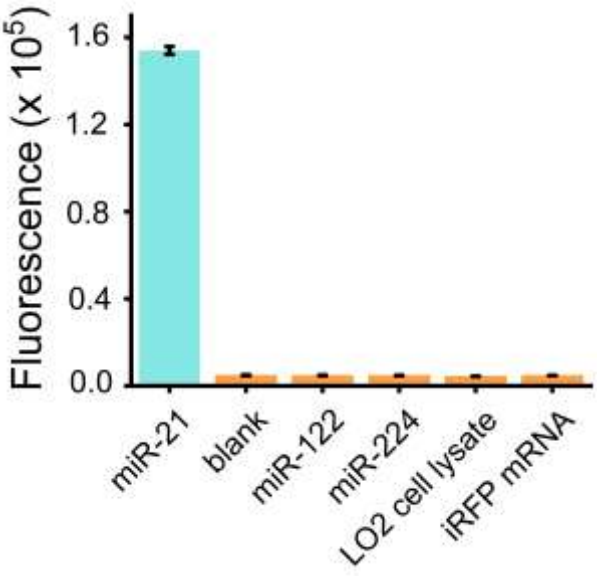

Figure S16. Selectivity study for 16× NP mi21LS. Fluorescence intensities of miLS at λ_{em}=530 nm to different substances.

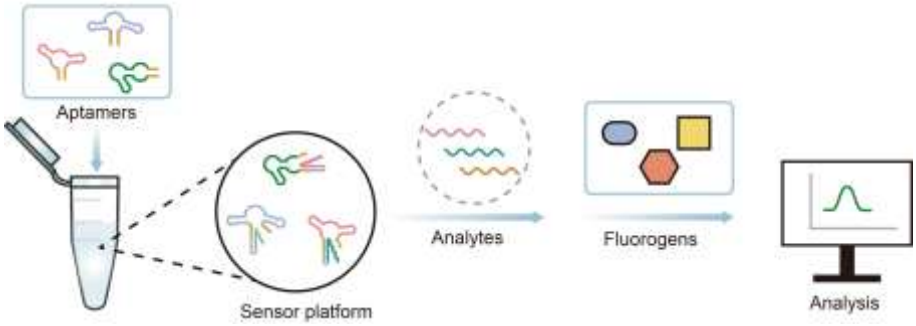

Figure S17. Schematic illustration of miLS platform for multiplex target and different aptamer.

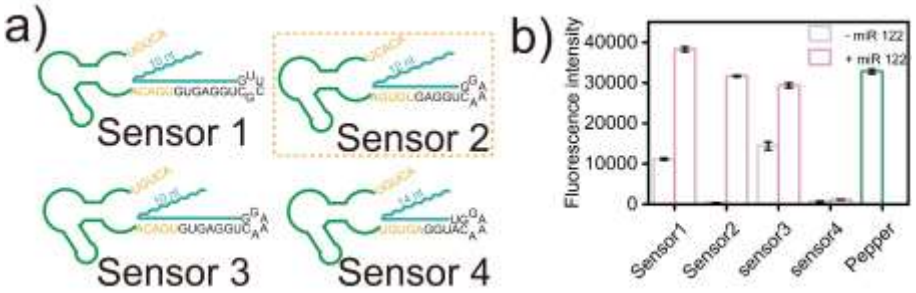

Figure S18. (a) Schematic for the optimization of NP mi122LS, containing the toehold sequence length is denoted by cyan lines, P1 stem sequence is marked by yellow bases, and tetraloop UUCG or GAAA. (b) Fluorescence intensity for optimizing NP mi122LS based on different sequence designs in (a). Data represent means ± SD, n=3.

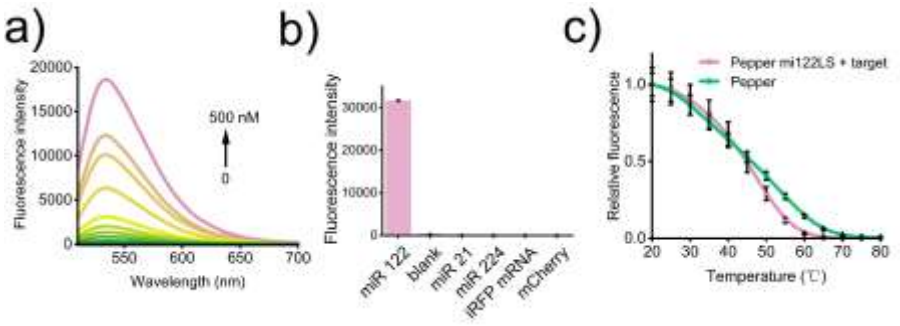

Figure S19. (a) Fluorescence spectra of the optimal NP mi122LS in the presence of HBC530 loaded with different concentrations of miR-122. (b). Selectivity study for NP mi122LS. Fluorescence intensities of miLS at λ_{em}=530 nm to different substances. (c) Temperature-dependence relative fluorescence intensity of NP mi122LS with target and Pepper aptamer with 5 μM HBC530. Data represent means ± SD, n=3. Relative fluorescence is defined as the ratio of the fluorescence value to the maximum fluorescence.

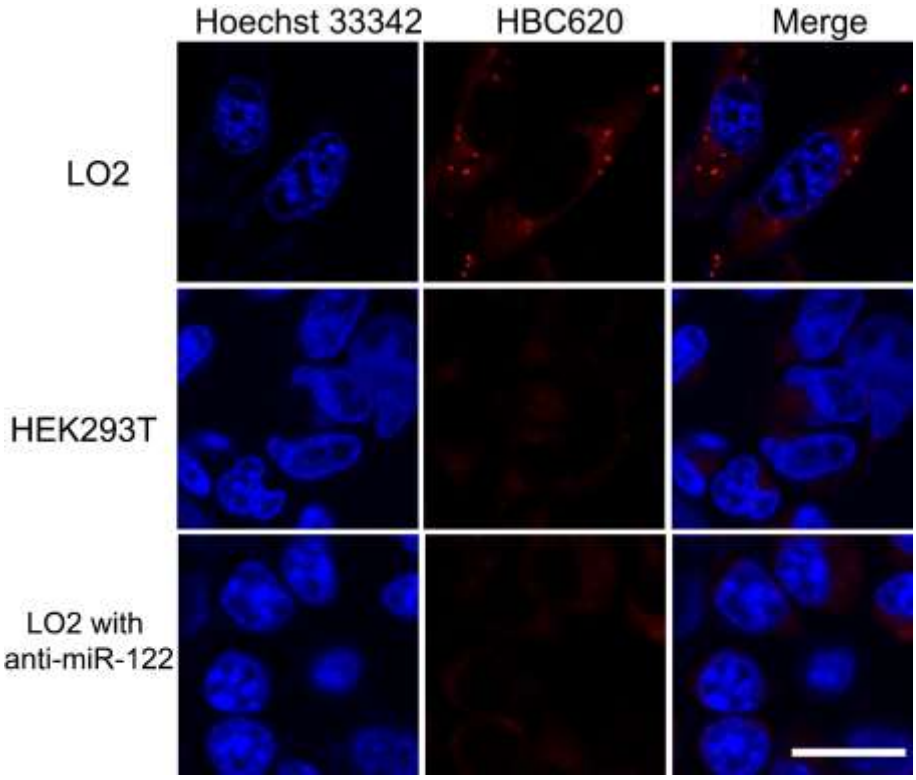

Figure S20. Confocal imaging results of the LO2, HEK293T and LO2 with anti-miR-122 cell line transfected the fluorogenic NP mi122LS system when incubated with HBC620. Scale bar, 20 μm.

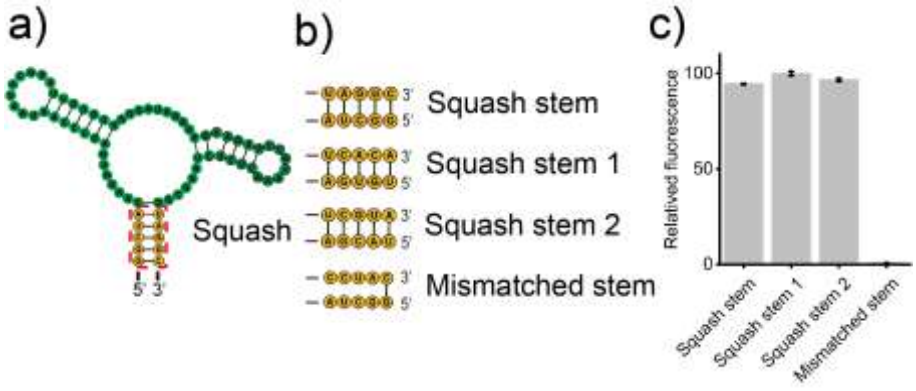

Figure S21. (a) The predicted secondary structure of a minimized Squash sequence with stem circled by a red box. The structure was generated using RNA Structure. (b) Mutation analysis of stem of Squash. The Stem of the Squash was replaced by either of the three randomly selected stems of different sequences. The "mismatched stem" retains the original AUCGG found in Squash but replaces the stem with four mismatched nucleotides to prevent duplex formation. (c) Relative fluorescence of Squash with a different stem. Data was repeated three times. Relative fluorescence is defined as the ratio of the fluorescence value to the maximum fluorescence.

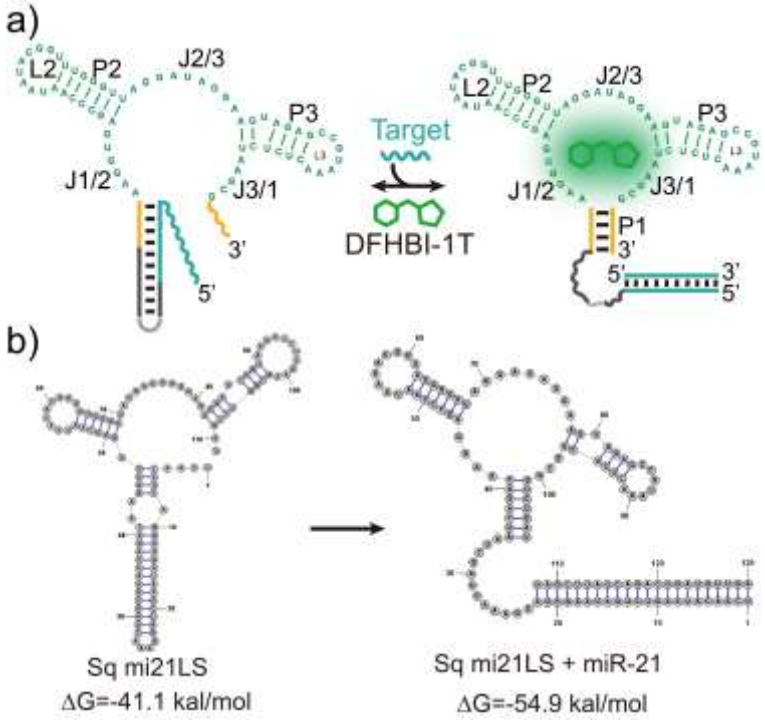

Figure S22. (a) Schematic illustration of the working principle for Sq mi21LS. Green bases denote the Squash, the yellow lines represent the P1 of the Squash, and the cyan lines show the target binding region. (b) The predicted secondary structure of Sq mi21LS and Sq mi21LS with the target. The structure was generated using *RNA Structure* software.

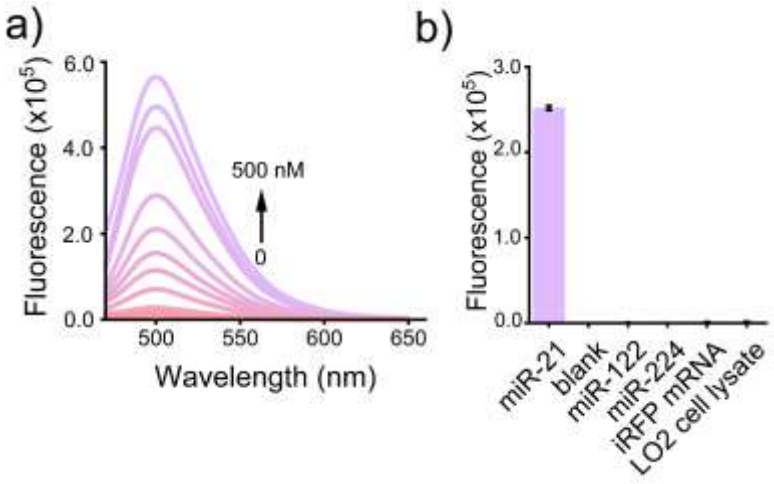

Figure S23. (a) Fluorescence spectra of the optimal Sq mi21LS in the presence of DFHBI-1T loaded with different concentrations of miR-21. (b) Selectivity study for Sq mi21LS. Fluorescence intensities of miLS at λ_{em}=500 nm to different substances.

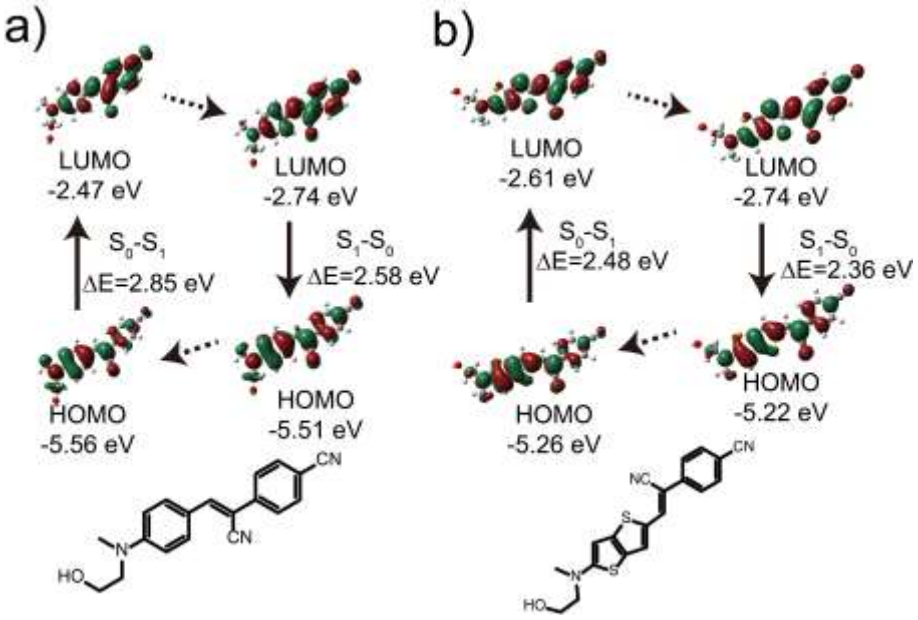

Figure S24. Frontier molecular orbital plots of (a) HBC530 and (b) HBC620 in water involved in the vertical excitation (left column) and emission (right column). The vertical excitation-related calculations are based on the optimized geometry of the ground state (S0), and the emission-related calculations are based on the optimized geometry of the excited state (S1). Excitation and radiative processes are marked as solid lines, and dotted lines mark the non-radiative processes.

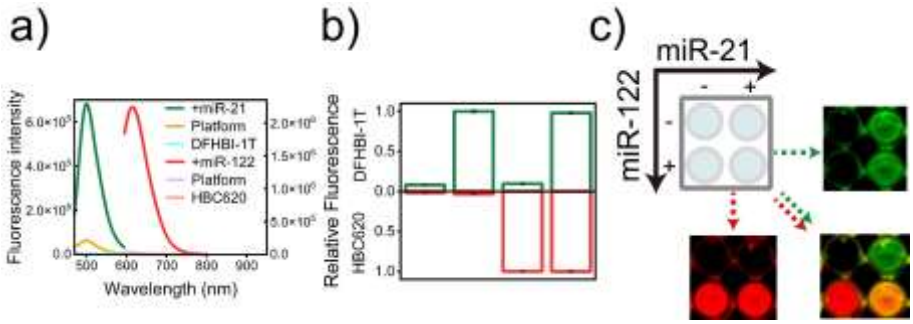

Figure S25. (a) Fluorescence spectra of miR-21 or miR-122 in the presence of dual-color miLS with DFHBI-1T and HBC620. (b) Relative fluorescent intensity of DFHBI-1T or HBC620 in the presence of orthogonal dual-color fluorogenic miLS system with different target RNA. Error bars are standard deviations in three repetitive assays. Relative fluorescence is defined as the ratio of the fluorescence value to the maximum fluorescence. (c) Imaging of the orthogonal dual-color miRNA dependent orthogonal imaging in a 96-well plate.

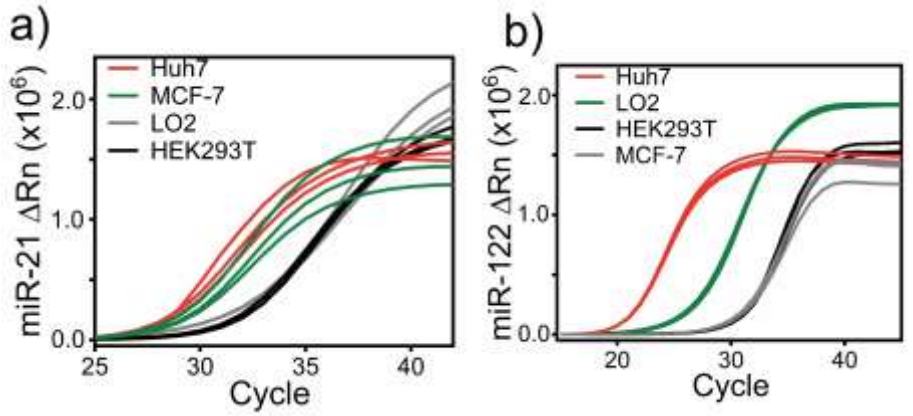

Figure S26. (a) qRT-PCR of miR-21 (b) miR-122 in Huh7, MCF-7, LO2 and HEK293T cells.

4. NMR Spectra

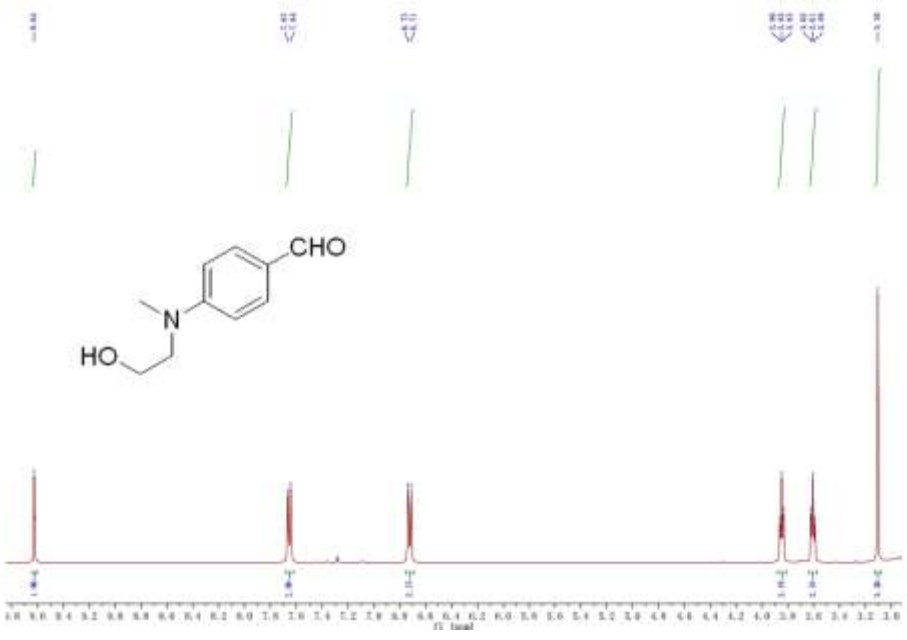

^{1}H NMR spectrum of Compound **1** in $CDCl_3$

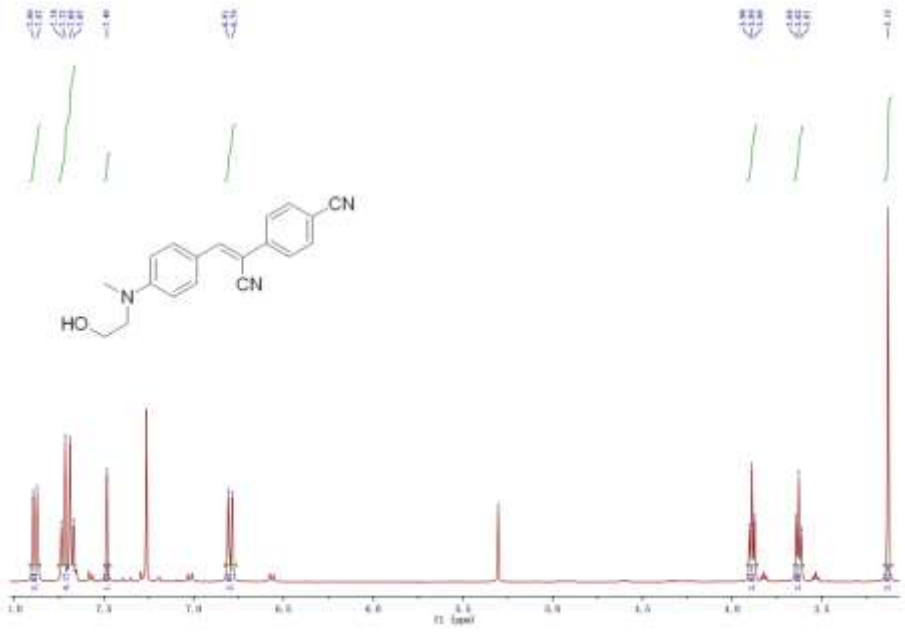

^{1}H NMR spectrum of HBC530 in $CDCl_3$.

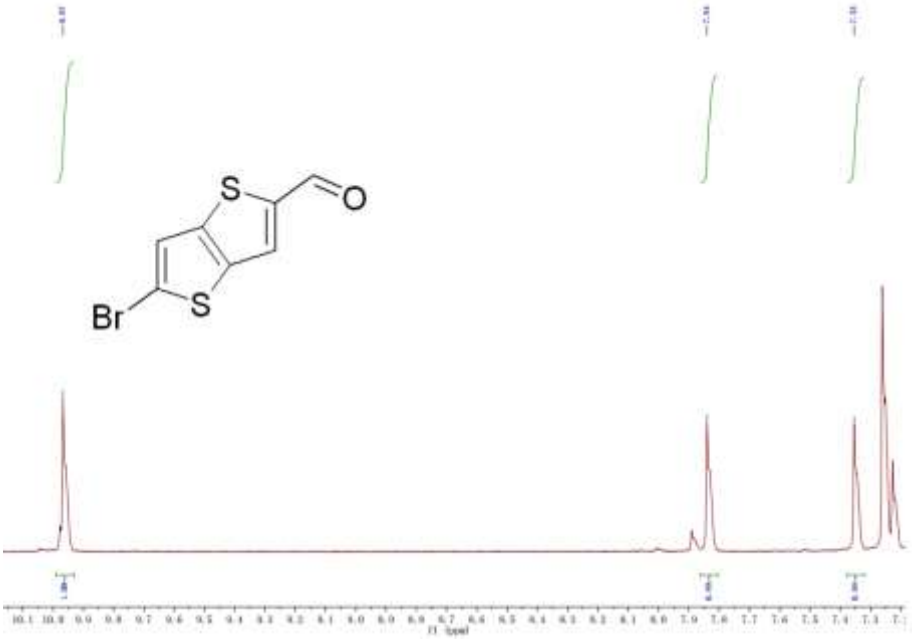

^{1}H NMR spectrum of Compound **2** in $CDCl_3$.

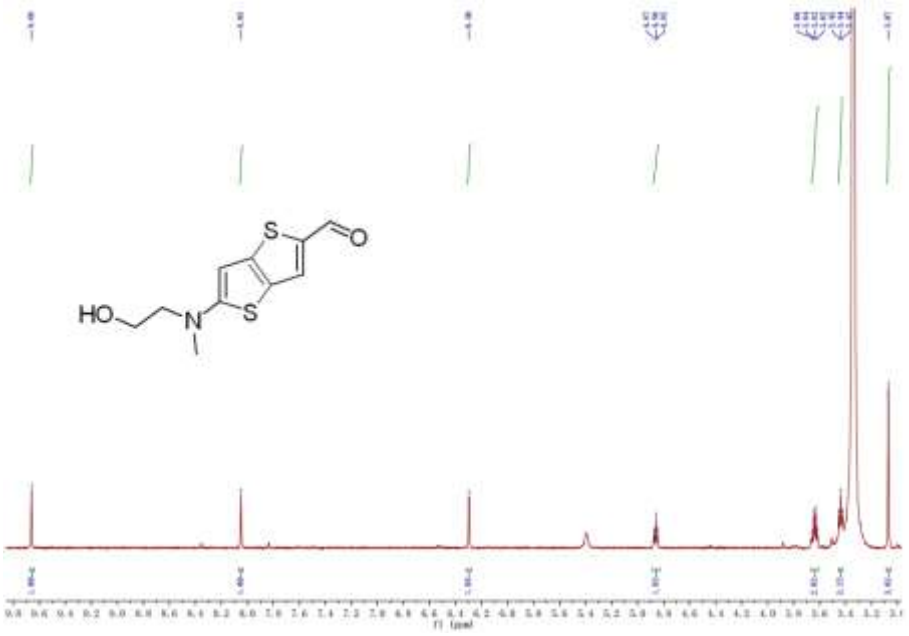

^{1}H NMR spectrum of Compound **3** in DMSO-d6.

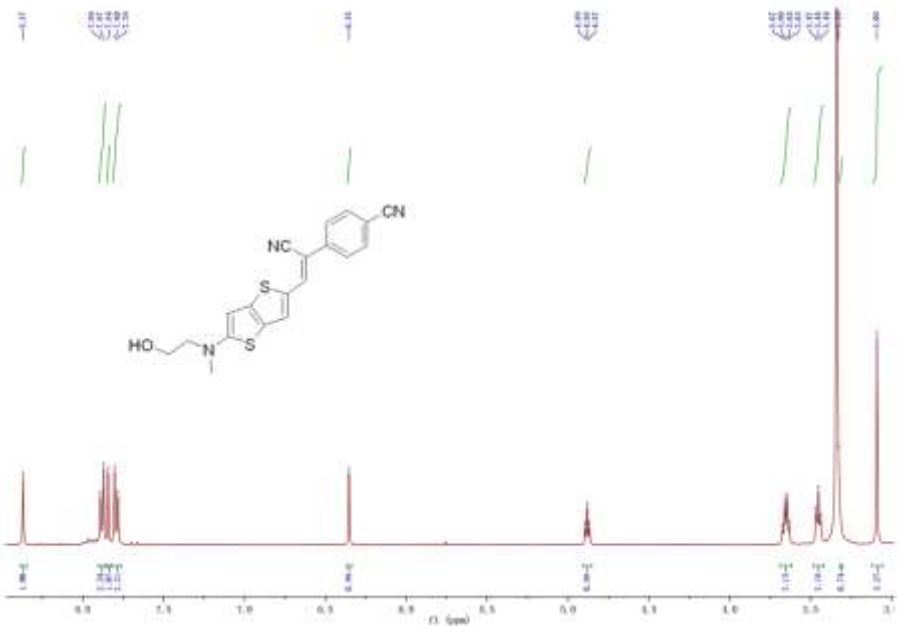

^{1}H NMR spectrum of HBC620 in DMSO-d6.

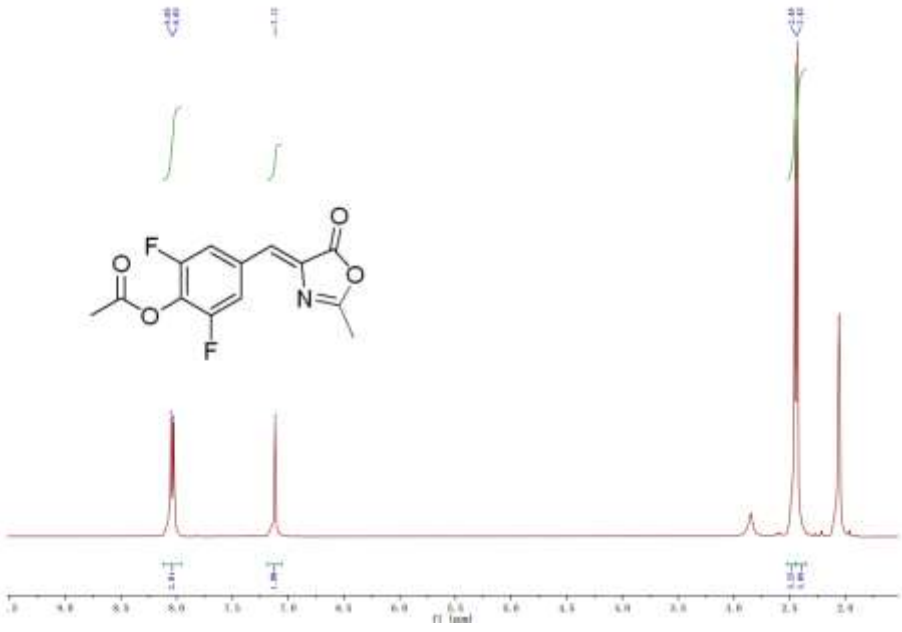

^{1}H NMR spectrum of Compound **4** in $CDCl_3$.

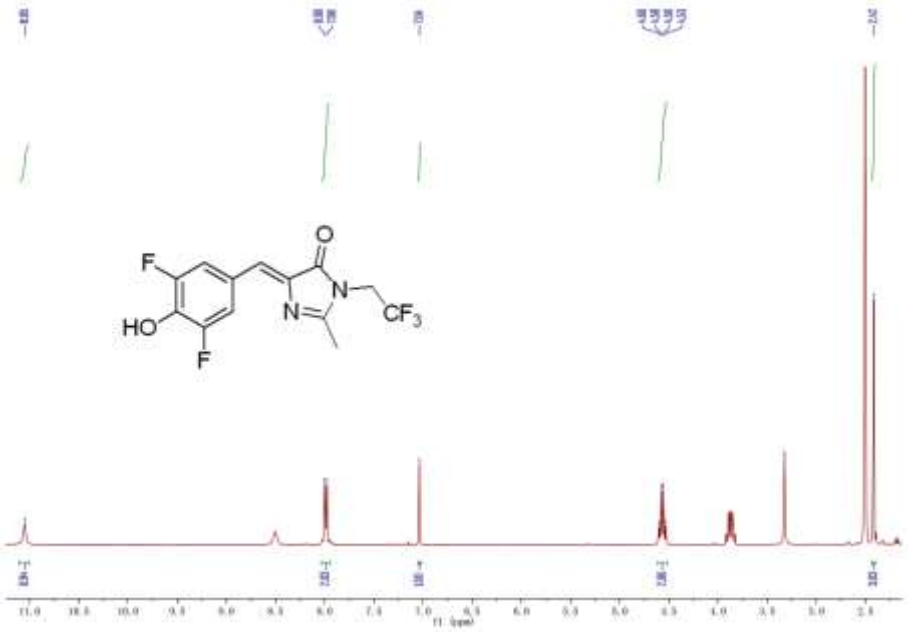

^{1}H NMR spectrum of DFHBI-1T in DMSO-d6.

5. References

1. Chen,X., Zhang,D., Su,N., Bao,B., Xie,X., Zuo,F., Yang,L., Wang,H., Jiang,L., Lin,Q., *et al.* (2019) Visualizing RNA dynamics in live cells with bright and stable fluorescent RNAs. *Nature Biotechnology*, **37**, 1287–1293.

2. Hu,X., Cai,S., Tian,G., Li,X., Su,J. and Li,J. (2013) Rigid triarylamine-based D–A–π–A structural organic sensitizers for solar cells: the significant enhancement of open-circuit photovoltage with a long alkyl group. *RSC Adv.*, **3**, 22544–22553.

3. Song,W., Strack,R.L., Svensen,N. and Jaffrey,S.R. (2014) Plug-and-Play Fluorophores Extend the Spectral Properties of Spinach. J. Am. Chem. Soc., 136, 1198–1201.

4. Trott,O. and Olson,A.J. (2010) AutoDock Vina: Improving the speed and accuracy of docking with a new scoring function, efficient optimization, and multithreading. *Journal of Computational Chemistry*, **31**, 455–461.

5. Huang,K., Doyle,F., Wurz,Z.E., Tenenbaum,S.A., Hammond,R.K., Caplan,J.L. and Meyers,B.C. (2017) FASTmiR: an RNA-based sensor for in vitro quantification and live-cell localization of small RNAs. *Nucleic Acids Research*, **45**, e130–e130.

6. Aw,S.S., Tang,M.X., Teo,Y.N. and Cohen,S.M. (2016) A conformation-induced fluorescence method for microRNA detection. *Nucleic Acids Research*, **44**, e92–e92.

7. Ying,Z.-M., Wu,Z., Tu,B., Tan,W. and Jiang,J.-H. (2017) Genetically Encoded Fluorescent RNA Sensor for Ratiometric Imaging of MicroRNA in Living Tumor Cells. *J. Am. Chem. Soc.*, **139**, 9779–9782.

8. Dou,C.-X., Liu,C., Ying,Z.-M., Dong,W., Wang,F. and Jiang,J.-H. (2021) Genetically Encoded Dual-Color Light-Up RNA Sensor Enabled Ratiometric Imaging of MicroRNA. *Anal. Chem.*, **93**, 2534–2540.

9. Dou,C.-X., Ying,Z.-M., Tang,L.-J., Wang,F. and Jiang,J.-H. (2022) Genetically Encoded Light-Up RNA Amplifier Dissecting MicroRNA Activity in Live Cells. *Anal. Chem.*, **94**, 15481–15488.